

Determining the contribution of mandibular dysmorphology to cleft palate in Pierre Robin sequence

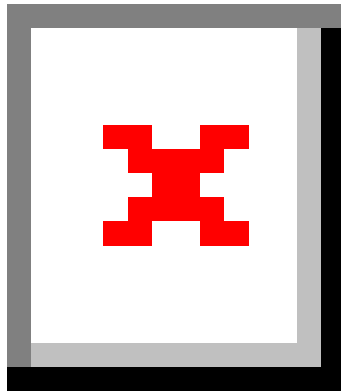
2023 Biomedical Research Awards (BRA)

Dr. Alice Goodwin

afg49@pitt.edu
O: 412-648-7412

FollowUp Form

Award Information



In an attempt to make things a little easier for the reviewer who will read this report, please consider these two questions before this is sent for review:

- Is this an example of your very best work, in that it provides sufficient explanation and justification, and is something otherwise worthy of publication? (We do publish the Final Report on our website, so this does need to be complete and polished.)*
- Does this Final Report provide the level of detail, etc. that you would expect, if you were the reviewer?*

Title of Project:*

Determining the contribution of mandibular dysmorphology to cleft palate in Pierre Robin sequence

Award Type

Biomedical Research Award (BRA)

Period of AAOF Support

July 1, 2023 through June 30, 2024

Institution

University of Pittsburgh-Of the Commonwealth System of Higher Education

Names of principal advisor(s) / mentor(s), co-investigator(s) and consultant(s)

Andrew Jheon

Amount of Funding

\$40,000.00

Abstract

(add specific directions for each type here)

Please find Abstract attached.

Respond to the following questions:

Detailed results and inferences:*

If the work has been published, please attach a pdf of manuscript below by clicking "Upload a file".

OR

Use the text box below to describe in detail the results of your study. The intent is to share the knowledge you have generated with the AAOF and orthodontic community specifically and other who may benefit from your study. Table, Figures, Statistical Analysis, and interpretation of results should also be attached by clicking "Upload a file".

AAOF BRA Final Report Manuscript Goodwin Dec 2024.pdf

Please find manuscript and figures based on the BRA work to be submitted for publication by February 2025 attached.

Comment: The AAOF PARC commends you on completing your proposed studies and for the contribution these findings make to advancing craniofacial genetics and the orthodontic specialty. We look forward to your future publications and endeavors.

Were the original, specific aims of the proposal realized?*

Yes, the original specific aims of the proposal were achieved.

Aim 1: Determine the contribution of mandibular dysmorphology to clefting of the secondary palate in PRS. We hypothesized that loss of Sox9 in the mandibular mesenchyme only would result in a hypoplastic and retrognathic mandible that physically blocked palatal shelf elevation and caused cleft palate, in the absence of palatal shelf defects. This hypothesis proved true. We deleted Sox9 specifically in the mandibular mesenchyme with our Hand2Cre driver and found that the Sox9fl/fl;Hand2Cre embryos had a fully penetrant, complete cleft of the secondary palate. We assessed the mandible and tongue morphology and position via histology and by measuring the distance between the tongue and skull. We found that due to the retrognathic mandible, the tongue was positioned in the inter-palatal shelf space throughout palatogenesis. Thus, we hypothesized that it was the retrognathic tongue position due to the retrognathic mandible that physically blocked palatal shelf elevation, resulting in cleft palate in our Sox9fl/fl;Hand2Cre mouse model. In order to distinguish between the contribution of the mandible vs tongue malposition to cleft palate in PRS, we generated a DTA;Hand2Cre model (in which every cell that expressed Hand2Cre would express diphtheria toxin and undergo apoptosis) that had both micrognathia and microglossia. Interestingly, the majority of the DTA;Hand2Cre embryos collected formed a normal palate since the palatal shelves developed horizontally, superior to the inferiorly positioned tongue, providing further evidence of the importance of tongue malposition to cleft palate in PRS.

Aim 2: Analyze the role of Sox9 in specification of the mandibular mesenchyme, cartilage development, and osteogenesis. We hypothesized that loss of Sox9 in the mandibular mesenchyme would result in disruption of specification of mesenchymal cells, with a shift away from the cartilage lineage to the osteoblast lineage, resulting in loss of the developing Meckel's cartilage (MC) and premature ossification of the mandibular bone, contributing to the shortening of the mandible in the antero-posterior dimension. We first quantified the shape differences caused by loss of Sox9 in the mandibular mesenchyme by analyzing uCT of Sox9fl/fl;Hand2Cre and control embryos at E18.5 and found the mandibular bone was smaller and malformed with decreased bone volume and alterations in mineralization in the mutant compared to control. We also measured the MC and found that it initiated development but did not elongate in the mutant. This arrest in MC development was accompanied by significant reduction in proliferation in the the MC of the mutant compared to control. To further understand the MC and mandibular bone phenotype we assessed expression patterns and levels of cartilage and osteoblast genes and found that there was a significant decrease in cartilage markers (Col2a1 and Acan), increase in early osteoblast marker (Runx2), and decrease in mature osteoblast markers (Ibsp and Sp7) in the mutant compared to control, suggesting a shift from the chondrogenic to osteogenic lineage with disruption of maturation of the osteoblasts. Finally, to determine downstream targets of Sox9 in mandibular development, we performed RNA seq on RNA extracted from the mandible (with tongue removed) at E14.5 from Sox9fl/fl;Hand2Cre and control embryos. We identified 19 significantly, differentially expressed genes. 10/19 genes were known target/interacting factors of Sox9 which provided proof of the validity of our experiment. There were also interesting novel genes with yet unknown roles in mandibular development. Six6 was the most differentially expressed gene (decreased in mutant compared to control), and we are currently determining the role of Six6 in craniofacial development by deleting it in the mandibular mesenchyme and exploring Six6 as a candidate gene in PRS by testing SNPs in a human population. This ongoing work based on the findings from the AAOF BRA is supported in part by the Bethel Musculoskeletal Family Center Fellowship (Oct 2024-Sept 2025).

Were the results published?*

No

Have the results of this proposal been presented?*

Yes

To what extent have you used, or how do you intend to use, AAOF funding to further your career?*

I have been very fortunate to receive and greatly appreciate funds from AAOF. I benefited greatly from the PFA that provided time and support for me as a postdoc to develop my research project, obtain NIDCR funding (K08), and attain a faculty position at UCSF. The BRA provided funds to support research projects in my lab at UCSF and Pitt (since September 2023), resulting in a funded grant from the Bethel Musculoskeletal Research Center (\$30,000 October 2024-September 2025). The BRA funds provided supplies and technical support to generate data for R03 applications as well as the attached manuscript based on the BRA work which will be submitted by February 2025. I plan to continue to apply for AAOF funding during my career with the goal of attaining additional funding to support my lab in order to advance research in the craniofacial/orthodontic field and ultimately impact patient care and orthodontic education.

Accounting: Were there any leftover funds?

\$0.00

Not Published

Are there plans to publish? If not, why not?*

Yes, the manuscript will be submitted by February 2025. I am currently finalizing data and revising the manuscript with co-authors.

Presented

Please list titles, author or co-authors of these presentation/s, year and locations:*

Mandible specific Sox9 loss results in cleft palate in Pierre Robin sequence mouse model; Caroline C. Chen, Nam Nguyen, Andrew H. Jheon, Jeffrey Bush, and Alice F. Goodwin; International Association for Dental Research (IADR) meeting, New Orleans, LA, March 2024, poster

Mandible specific Sox9 loss results in mandibular dysmorphology and cleft palate in a Pierre Robin sequence mouse model; Alice Goodwin; University of Missouri-Kansas City (UMKC) Oral and Craniofacial Sciences Seminar, May 15, 2024, talk

Contribution of Mandible vs Tongue Malposition in Pierre Robin Sequence Utilizing Mouse Models; Sushan Zhang, Caroline C. Chen, Nam Nguyen, Andrew H. Jheon, Jeffrey O. Bush, and Alice F. Goodwin; American Association for Oral, Dental, and Craniofacial Research (AADOCR) meeting, New York, NY, March 2025, poster

Was AAOF support acknowledged?

If so, please describe:

Yes, AAOF support was acknowledged during talks and on posters presented and will be acknowledged in the published manuscript.

Internal Review

Reviewer comments

Reviewer Status*

Approved

File Attachment Summary

Applicant File Uploads

- AAOF BRA Final Report Manuscript Goodwin Dec 2024.pdf

Mandible-specific loss of Sox9 leads to mandibular dysmorphology and cleft palate in a Pierre Robin sequence mouse model

Caroline C. Chen^{1*}, Sushan Zhang^{2,3*}, Nam Nguyen¹, Isabel Mangoba¹, Mya Blanco^{2,3}, Dakota Volzer^{2,3}, Christopher P. Chen¹, Darnell Cuylear¹, Andrew H. Jheon^{2,3}, Jeffrey Bush⁴, and Alice F. Goodwin^{2,3^}

¹Department of Orofacial Sciences, University of California San Francisco, School of Dentistry

²Department of Orthodontics and Dentofacial Orthopedics, University of Pittsburgh, School of Dental Medicine

³Center for Craniofacial Regeneration, University of Pittsburgh, School of Dental Medicine

⁴Department of Cell and Tissue Biology, University of California San Francisco, School of Dentistry

*Co-first authors

^Corresponding author:

Alice Goodwin DDS, PhD

Assistant professor, Department of Orthodontics and Dentofacial Orthopedics

University of Pittsburgh School of Dental Medicine

Email: afg49@pitt.edu

Phone: (412) 648-7412

Abstract:

Background: Pierre Robin sequence (PRS) is a triad of clinical findings that includes mandibular retrognathia, glossoptosis, and airway obstruction. The majority of individuals with PRS present with cleft palate, and isolated cases are associated with mutations in the regulatory and coding regions of *SOX9*. Here, we deleted *Sox9* specifically in the mandibular mesenchyme with our newly generated *mtHand2^{Cre}* mouse line to understand mandibular dysmorphology and its contribution to cleft palate in PRS. Additionally, we bred *R26R^{DTA};mtHand2^{Cre}* embryos with micrognathia and microglossia to determine the contribution of tongue malposition to clefting.

Results: Deletion of *Sox9* in the mandibular mesenchyme resulted in a hypoplastic, dysmorphic, and retrognathic mandible with decreased bone volume. The development of Meckel's cartilage was arrested, and there was misexpression of chondrogenic and osteogenic markers in the developing mandibular bone. Interestingly, there was a complete cleft of the secondary palate that was fully penetrant. In contrast, the majority of *R26R^{DTA};mtHand2^{Cre}* embryos formed a normal palate.

Conclusions: Here, we introduce our mandibular- and tongue-(mt) specific *mtHand2^{Cre}* mouse line. Moreover, we present *in vivo*, genetic evidence of the contribution of the mandible and tongue to cleft palate (in the absence of palate intrinsic mechanisms).

INTRODUCTION:

Pierre Robin sequence (PRS) is a triad of clinical findings that include mandibular retrognathia, glossoptosis, and airway obstruction. PRS is associated with cleft palate in 60-90% of cases.¹ PRS may present as an isolated condition or as part of a syndrome, which include Stickler (most common), 22q11 deletion, Duane, Cornelia de Lange, Mobius, and Nager syndromes.^{2,3} Isolated PRS is associated with loss of function mutations in regulatory and coding regions of *SOX9*.⁴⁻⁶ Clinically, the severity of isolated PRS varies, with infants with moderate to severe presentation requiring tracheostomy shortly after birth to establish airway and mandibular distraction osteogenesis in the first years of life to lengthen the mandible, as well as mandibular advancement in the teenage years to treat retrognathia.⁷⁻⁹ There are risks and morbidities associated with every surgical intervention. For instance, the complication rate of mandibular distraction osteogenesis in the PRS patient population is 34%, with most complications classified as minor or moderate, including device failure, hypertrophic scarring, and facial neuropraxia.⁹ However, major complications, such as TMJ ankylosis, facial nerve injury, dental injury, and death are reported in 9% of cases.⁹

The secondary palate and mandible develop concurrently and in coordination in humans and mice. The cranial neural crest cells (CNCCs) migrate from the dorsal aspect of the neural tube and populate the paired maxillary and mandibular prominences at ~4 weeks in human and embryonic (E) day 10.5 in mice.^{10,11} The palatal shelves develop from the maxillary processes, grow vertically, lateral to the developing tongue, and then reorient to a horizontal position dorsal to the tongue in a process termed palatal shelf elevation. After elevation, the shelves grow horizontally to meet at the midline and fuse to form the palate. At the same time, the mandibular prominences grow and fuse in the midline, and Meckel's cartilage (MC) forms eventually giving rise to the malleus and incus of the ear, as well as the sphenomandibular ligament in the proximal region and mandibular symphysis in the distal. The ventral portion of MC establishes the horseshoe-shaped primordia of the mandible and guides early morphogenesis, and then

ultimately, this portion of the MC disappears via apoptosis and autophagy.¹²⁻¹⁴ The body of the mandibular bone develops via intramembranous ossification lateral to the MC.

Retrusion of the mandible and tongue is thought to physically block palatal shelf elevation and contribute to cleft palate, and several genes have been implicated in clefting of the secondary palate with mandibular involvement in mice,¹⁵⁻¹⁷ including *Sox9*.^{18,19} However, much of the evidence to support this hypothesis was produced in tissue culture systems^{16,19,20} with significant caveats including cell death and tissue growth retardation.^{21,22} *In vivo* studies using tissue-specific drivers in mice have primarily utilized CNCC-^{23,24} or palatal shelf-specific^{25,26} Cre lines, and so it has been challenging to distinguish between palatal shelf intrinsic mechanisms and contributions of the surrounding tissue, including the mandible and tongue, in the pathogenesis of secondary palate clefting.

Here, we utilize a newly generated genetic tool, the mandible- and tongue- (mt) specific *mtHand2*^{Cre} mouse line, which drives Cre recombination specifically in the mandibular mesenchyme and not surrounding tissue, to further study mandibular development and its contribution to cleft palate in PRS. Deletion of *Sox9* in the mandibular mesenchyme only with *mtHand2*^{Cre} resulted in mandibular hypoplasia and a fully penetrant cleft of the secondary palate. The mandible was small, dysmorphic, and retrognathic with arrest of Meckel's cartilage elongation and disruption of osteoblast maturation. Furthermore, the retrognathic mandible and tongue remained in the space between the palatal shelves throughout palatogenesis in our *Sox9*^{fl/fl}; *mtHand2*^{Cre} PRS mouse model, resulting in delayed palatal shelf elevation and, ultimately, cleft palate. Moreover, we crossed *mtHand2*^{Cre} with *R26R*^{DTA}, generating a mouse model with micrognathia and microglossia. The majority of these mice did not develop cleft palate, highlighting the importance of both mandible and tongue malposition in contribution to cleft palate.

MATERIALS AND METHODS:

Mouse husbandry and generation of *Hand2*^{Cre} mouse

All experiments involving mice were conducted in accordance with protocols approved by the UCSF and University of Pittsburgh Institutional Animal Care and Use Committees. The *mtHand2^{Cre}* transgenic mouse was generated at the UCSF Transgenic Core via pronuclear injection of DNA containing the pharyngeal enhancer of *Hand2* (sequence generously provided by David Clouthier²⁷) upstream of a minimal promoter *Hsp68* and *Cre*. DNA (3656bp) injected into FVB/N embryos generated 41 founder mice (21 males and 20 females). Genotyping for *Cre* identified 9 *Cre*⁺ mice (5 males and 4 females). *Cre*⁺ mice were crossed with the *R26R^{mT/mT}* (*Gt(ROSA)26Sor^{tm4(ACTB-tdTomato,-EGFP)Luo}*) mouse line²⁸ to determine the *Cre* expression pattern, and embryos from one founder male showed mandibular specific *Cre* expression. This founder was crossed with B6 mice to establish the line. Other mouse lines utilized include *Sox9^{fl/fl}* (B6.129S7-*Sox9^{tm2Cm/J}*, JAX stock #013106²⁹) and *R26R^{DTA/DTA}* (*Gt(ROSA)26Sor^{tm1(DTA)Lky}*, JAX stock #009669³⁰).

Micro computed tomography and geometric morphometric analysis

For micro computed tomography (μ CT), E18.5 embryo heads were collected and fixed in 4% paraformaldehyde. Samples were scanned using a MicroCT50 (Scanco), 55kVp, 109 μ A, 6W at 20 μ m voxel size resolution. For geometric morphometric analysis (GMA), hemi-mandibles and crania were segmented and isosurfaces generated in Avizo software (Thermo Fisher Scientific). Landmarking (16 landmarks per hemi-mandible and 81 on cranium³¹) and GMA were completed in Checkpoint software (Stratovan). Bone volume and density were measured using Avizo software.

Histological analysis

Timed mating trios were set up, and presence of a vaginal plug was considered E0.5 at noon the following day. Pregnant dams were euthanized, and embryos collected, fixed in 4% paraformaldehyde, and genotyped. For MC analysis, entire embryos were stained with alcian blue, imaged with a Zeiss SteREO Discovery v12, and measurements were taken using open source Fiji software. For other histological analyses, embryonic heads were embedded in paraffin,

serially sectioned coronally at 7 μ m, and stained with hematoxylin and eosin. Immunohistochemistry was performed on cryosections (sectioned coronally at 5 μ m using a Leica cryostat) using antibodies against GFP (Abcam AB13970, 1:250) and Sox9 (R&D Systems #AF3075, 1:250). For proliferation analysis, pregnant dams were injected intraperitoneally with 1 mg of BrdU 1 hour prior to euthanasia, embryos were collected, paraffin processed, and stained using an antibody against BrdU (Abcam #6326, 1:500). Nuclei and BrdU-positive cells were quantified in the MC using Fiji and statistical significance was determined using Student's T-test. To assess cell death, TUNEL staining (In Situ Cell Death Detection Kit, Roche) was performed. RNAscope (ACD Diagnostics) was performed with mouse probes against *Col2a1* (407221), *Runx2* (414021), *Ibsp* (415501), and *Sp7* (403401). Sections were imaged on a Leica DMI8 or Nikon Eclipse TE2000-E microscope.

RESULTS:

***mtHand2*^{Cre} drives Cre recombination specifically in the mandibular mesenchyme**

The temporal and spatial activity of the *mtHand2*^{Cre} driver was tested by crossing it with a *R26R*^{mT/mT} reporter. Gross observation of the entire embryo showed the earliest *mtHand2*^{Cre} recombinase activity, as shown by GFP expression, was noted at E10, specifically in the developing pharyngeal arch 1 and no surrounding tissue (data not shown). *mtHand2*^{Cre} expression was specific to the first pharyngeal arch at E10.5 and became limited to the mandibular mesenchyme by E14.5 (Figure 1A,B). At E18.5, *mtHand2*^{Cre} expression was specific to the lower jaw (Figure 1C).

Upon closer examination in sections at E12.5, GFP was expressed in the *R26R*^{mT/+;mtHand2}^{Cre}

embryos in the developing mandible and tongue, and not the palatal shelves (Figure 1D-D"). The expression pattern in the mandibular mesenchyme was consistent along the antero-

posterior axis at E12.5. At E14.5, GFP was observed in the tongue, mandible, and MC throughout the antero-posterior axis (Figure 1E-E"). In the posterior region, there was no GFP in the palatal shelves (Figure 1E"), however, in the middle and more so in the anterior region, GFP expression was observed in a subset of the palatal shelf cells (Figure 1E-E'). At E18.5, GFP expression was present in the tongue, mandibular bone, and MC; GFP was not expressed in the ossifying secondary palate (Figure 1F-F"). Of note, *mtHand2^{Cre}* was not expressed in the molar dental mesenchyme (Figure 1E'F'); however, it was expressed in the incisor mesenchyme (Figure 1F). Finally, we demonstrated *mtHand2^{Cre}* functionally alters gene expression specifically in the mandibular mesenchyme by deleting *Sox9* with *mtHand2^{Cre}*. In *Sox9^{fl/fl};mtHand2^{Cre}* embryos, *Sox9* expression was lost in the MC at E13.5 and E14.5 whereas the expression persisted in tissues outside of the mandibular mesenchyme, including the cranial base, nasal cartilages, and molar epithelium (Supplemental Figure 1).

Deletion of *Sox9* in the mandibular mesenchyme only results in a hypoplastic, dysmorphic, and retrognathic mandible

Isosurfaces generated from μ CT data on *Sox9^{fl/fl};mtHand2^{Cre}* mutant and control skulls at E18.5 show the mandible was hypoplastic and dysmorphic as well as retrognathically positioned relative to the maxilla in the mutant compared to control (Figure 2A,B). Geometric morphometric analysis (GMA) was performed to quantify the shape difference of *Sox9^{fl/fl};mtHand2^{Cre}* mutant hemi-mandibles (N=8) compared to control (N=6) at E18.5. First, centroid size analysis revealed that the mandibular body was significantly smaller in the *Sox9^{fl/fl};mtHand2^{Cre}* mutant embryos compared to control (Supplemental Figure 2). Next, GMA on *Sox9^{fl/fl};mtHand2^{Cre}* mutant and control embryos at E18.5 revealed significant shape differences as control and mutant samples separated along principle component (PC) 1 and 2, accounting for 58.99% and 16.12% of the shape variation, respectively (Figure 2C). The shape differences were primarily noted in the proximo-dorsal length and ventro-dorsal width of the mandible, as well as the angulation of the condylar and angular processes, as shown by the wireframes representing PC1 max, PC1 min,

and average (Figure 2D). Finally, bone volume and mineral density of the mandibular bone were analyzed. The volume of the mandibular bone was decreased in the *Sox9^{fl/fl};mtHand2^{Cre}* embryos at E18.5 compared to control, and relative bone mineral density heat maps show the mineralization pattern was altered in the mutant compared to control (Figure 2E-G).

Loss of Sox9 in the mandibular mesenchyme results in truncation of Meckel's cartilage with decreased proliferation and disruption of osteoblast differentiation in the mandibular bone

To further understand the mandibular dysmorphogenesis in the *Sox9^{fl/fl};mtHand2^{Cre}* embryos, we evaluated MC development. Skeletal preps of *Sox9^{fl/fl};mtHand2^{Cre}* and control embryos at E13.5 and E14.5 showed the MC was significantly shorter in the mutant compared to control (Figure 3A-D, K). At E13.5, the control MC was 2.24mm vs 0.55mm in mutants; at E14.5, control MC was 2.77mm vs 1.08 mm in mutants (Figure 3A-D, K). In addition, while the MC length in the control increased significantly from E13.5 to E14.5, the change in mutant MC length was not significant, suggesting that MC development was initiated in the *Sox9^{fl/fl};mtHand2^{Cre}* embryos, but development did not progress, resulting in a truncated MC (Figure 3K). Furthermore, the cross-sectional area of the MC was significantly decreased in the mutant compared to control at E12.5, E13.5, and E14.5 (Figure 3E-J). Control MC area increased significantly from E12.5 to E14.5, whereas no significant difference was observed in the mutant (Supplemental Figure 3A).

The truncation of the MC in *mtSox9^{fl/fl};Hand2^{Cre}* embryos was accompanied by decreased proliferation in the MC. The percentage of BrdU-positive or proliferative cells was significantly decreased in mutants compared to controls at E12.5 (23.45% control vs 10.57% mutant), E13.5 (27.42% control vs 10.33% mutant), and E14.5 (28.28% control vs 8.11% mutant; Figure 3E-J, L). There was a significant difference in apoptosis, as measured by the number of TUNEL-positive cells in the area of the MC (including the perichondrium as indicated by orange dashed line in Figure 3G-J) at E13.5. Mutants showed 0.07% TUNEL-positive cells compared to 0.04% in

controls at E13.5 but no significant differences were observed at E12.5 or E14.5 (Supplemental Figure 3B).

To further understand the disruption in chondrogenesis and osteogenesis in the mandible of *Sox9^{fl/fl};mtHand2^{Cre}* embryos, chondrogenic and osteogenic markers were evaluated. At E12.5, prior to MC and mandibular bone development, *Col2a1*, a marker of chondrocytes, was expressed in the condensing mandibular mesenchyme in the region where the MC forms in the control embryo, and *Col2a1* expression was significantly reduced in this region in the *Sox9^{fl/fl};mtHand2^{Cre}* embryo (Supplemental Figure 4A,B). *Runx2*, a marker of pre-osteoblasts, was expressed broadly and at similar levels in the mandibular mesenchyme in both mutant and control embryos at E12.5 (Supplemental Figure 4C,D). At E14.5, *Col2a1* was expressed in the MC in the control embryos and absent in the *Sox9^{fl/fl};mtHand2^{Cre}* MC (Figure 3M,N). At E14.5, *Runx2* was primarily expressed lateral to the MC in the developing mandibular bone in control, whereas *Runx2* was expressed more broadly in the developing mandible and medial to the MC in the mutant (Figure 3O,P). There was a decrease in markers of mature osteoblasts. Both *Sp7* and *Ibsp* were expressed throughout the developing mandibular bone in control at E14.5, whereas *Sp7* and *Ibsp* expression was decreased in mutants with *Ibsp* expression limited to the dorsal aspect of the mandibular body (Figure 3Q-T).

***Sox9^{fl/fl};mtHand2^{Cre}* embryos have a fully penetrant cleft of the secondary palate and palatal shelf elevation delay**

Interestingly, with loss of *Sox9* in the mandibular mesenchyme only (and not palatal shelves and surrounding tissue), there was a complete cleft of the bones of the secondary palate in the *Sox9^{fl/fl};mtHand2^{Cre}* embryos (Supplemental Figure 5). This cleft was 100% penetrant in the samples collected (N=13: 1 at P0, 8 at E18.5, 4 at E16.5). The hypoplastic, retrognathic mandible and malpositioned tongue in *Sox9^{fl/fl};mtHand2^{Cre}* embryos appeared to obstruct palatal shelf elevation. At E13.5, the shape of the palatal shelves was similar in the *Sox9^{fl/fl};mtHand2^{Cre}* and control embryos (Figure 4A-B"). At E14.5, while the palatal shelves elevated to the horizontal

position and began to fuse, with the medial epithelial seam undergoing degeneration in the control embryos, the palatal shelves in the mutant were in the vertical orientation and had not elevated (Figure 4C-D"). Indeed, of the 22 E14.5 *Sox9^{fl/fl};mtHand2^{Cre}* embryos examined, the palatal shelves were not elevated in the vertical position in 91% (N=20) and elevated (in the horizontal position) in 9% (N=2), compared to 27 control embryos examined in which 7% (N=2) were not elevated, 18% (N=5) were elevated, and 74% (N=20) were adhered or fused, suggesting palatal shelf elevation was significantly delayed in *Sox9^{fl/fl};mtHand2^{Cre}* embryos compared to control (Figure 4G). By E16.5, the secondary palate was fused in the control, however, in the mutant, there was a cleft of the secondary palate along the entirety of the antero-posterior axis (Figure 4E-F"). Of note, the tongue was positioned in the inter-palatal shelf space in *Sox9^{fl/fl};mtHand2^{Cre}* embryos along the entire AP axis at E14.5 and E16.5 (Figure 4D-D",F',F"). The tongue position was determined by measuring the distance between the dorsal surface of the tongue to the skull (the cranial base in posterior sections and nasal floor in the anterior and middle regions). As expected, there was no significant difference in the distances along the antero-posterior axis at E13.5 (data not shown), however, at E16.5, the distances between the tongue and skull landmarks were significantly decreased in *Sox9^{fl/fl};mtHand2^{Cre}* embryos compared to control (Figure 4H). The cleft of the secondary palate was present at birth, and the tongue was positioned in the cleft (Supplemental Figure 6).

Palatal shelves fuse in the majority of *R26R^{DTA/+};mtHand2^{Cre}* embryos with micrognathia and microglossia

To further probe the mandible and tongue dimension and position that contribute to cleft of the secondary palate, we crossed *mtHand2^{Cre}* males with *R26R^{DTA/DTA}* females to generate *R26R^{DTA/+};mtHand2^{Cre}* embryos in which diphtheria toxin was expressed in all *mtHand2^{Cre}*-positive cells, causing death of these cells.³⁰ Phenotypically, the *R26R^{DTA/+};mtHand2^{Cre}* embryos had significant micrognathia (Figure 5A,B) and microglossia, with a small, inferiorly positioned tongue (Figure 5D-E"). Other than the craniofacial defects specific to the mandibular mesenchyme

derived tissues, the remainder of the embryo bodies appeared grossly normal (Supplemental Figure 7). At E16.5 the palatal shelves fused in the control embryos (Figure 5C-C") and in the majority of the $R26R^{DTA/+};mtHand2^{Cre}$ embryos (N=5/8; Figure 5D-D"). However, 3 out of 8 of the $R26R^{DTA/+};Hand2^{Cre}$ embryos collected at E16.5 had a cleft (Figure 5E-E"). In these $R26R^{DTA/+};mtHand2^{Cre}$ embryos with cleft, the tongue was in the inter-palatal shelf space as quantified by the decreased distance between the dorsal of the tongue and skull.

DISCUSSION:

Here, we utilized our newly generated $mtHand2^{Cre}$ to delete *Sox9* specifically in the mandibular mesenchyme, resulting in a small, dysmorphic mandible and cleft of the secondary palate with total penetrance that phenocopies the human condition of PRS. With the loss of *Sox9* in the mandibular mesenchyme, the development of the MC was arrested with decreased proliferation. There was also a shift from the chondrocyte to osteoblast lineage, however, mature osteoblast makers were expressed at decreased levels in the developing mandibular bone, suggesting a defect in osteoblast differentiation. The mandible and tongue in $Sox9^{fl/fl};mtHand2^{Cre}$ embryos were positioned in the inter-palatal shelf space throughout palatogenesis, and palatal shelf elevation was delayed, ultimately resulting in cleft palate. In comparison, the majority of $R26R^{DTA/+};mtHand2^{Cre}$ embryos with micrognathia and microglossia showed fusion of the palatal shelves.

First, we introduced our newly generated $mtHand2^{Cre}$, which drives Cre under the control of the pharyngeal enhancer of *Hand2* only, specifically in the mandibular mesenchyme. Our $mtHand2^{Cre}$ is an additional mouse line that complements the *dHand-Cre* mouse line in which the Cre is controlled by the pharyngeal and cardiac enhancers of *Hand2*, driving recombination in both the mandibular mesenchyme and cardiac tissue.²⁷ Although *dHand-Cre* has been useful in the mandibular-specific alteration of genes, its use is limited due to embryonically lethality from heart-specific effects. In these instances in which alteration of a gene that may affect cardiac

development, our *mtHand2^{Cre}* will prove to be especially useful. For example, we demonstrated here the utility of our *mtHand2^{Cre}* by crossing it to *R26R^{DTA/DTA}* which surely would have been embryonic lethal with expression in the heart with the *dHand-Cre*. Thus, our *mtHand2^{Cre}* provides an additional tool to the craniofacial biology field in the study of mandible and tongue development. Of note, there is some expression of the Cre in the anterior palate at E14.5, which should be considered and may be useful as an anterior palatal shelf Cre later in palatogenesis.

Next, we utilized *mtHand2^{Cre}* to specifically delete *Sox9* in the mandibular mesenchyme, successfully generating a useful PRS mouse model to further study this human condition. The mandibular bone was dysmorphic and retrognathic in *Sox9^{fl/fl};mtHand2^{Cre}* embryos, similar to the *Sox9^{fl/fl};Wnt1^{Cre}* mouse model. Unlike *Sox9^{fl/fl};Wnt1^{Cre}*, in which the MC did not form,³² the MC initiated development in the *Sox9^{fl/fl};mtHand2^{Cre}* embryo, however, MC development was arrested at E13.5. The significant decrease in proliferation observed at E12.5-E14.5 was likely a major contributing factor to both the decreased sectional area and arrest in elongation of the MC. In addition, the loss of *Sox9* may have shifted the specification of the osteochondroprogenitor cells in the mandibular mesenchyme from the chondrocyte to osteoblast lineage. In the axial skeleton, *Sox9* specifies the pool of osteochondroprogenitor cells, initiating the chondrocyte differentiation program and repressing osteoblast differentiation by inducing the expression of *Col2a1*, *Col2a2*, and *Aggrecan*, and repressing *Runx2*.^{29,33,34} Similarly, with loss of *Sox9* in the mandibular mesenchyme, there was loss of chondrocyte markers including *Col2a1* and *Acan* (data not shown) in the mandibular tissue of *Sox9^{fl/fl};mtHand2^{Cre}* embryos as early as E12.5 and at E14.5, whereas there was broadened expression of early osteoblast makers, including *Runx2* at E14.5. However, expression of mature osteoblast markers including *Sp7* and *Ibsp* was decreased at E14.5, suggesting osteoblast differentiation did not progress properly, which may have contributed to the mandibular bone phenotype of hypoplasia and disrupted mineralization. How the loss of *Sox9* and disruption of MC formation may affect mandibular bone formation, which undergoes intramembranous ossification, is not understood and requires further study.

Interestingly, the loss of *Sox9* in the mandibular mesenchyme in *Sox9^{fl/fl};mtHand2^{Cre}* embryos resulted in a cleft of the secondary palate that was fully penetrant. The *Sox9^{fl/fl};mtHand2^{Cre}* mouse model is the first to our knowledge to provide *in vivo*, genetic evidence of the contribution of mandibular dysmorphology to clefting of the secondary palate in the absence of palatal intrinsic mechanisms. Since *Sox9* is not expressed in the developing tongue, and the tongue size in cross section was normal in the *Sox9^{fl/fl};mtHand2^{Cre}* embryos, the problem appeared to be a normal sized tongue on a hypoplastic and retrognathic mandible. The tongue was thus positioned posteriorly and superiorly in the inter-palatal shelf space. In comparison, the *R26R^{DTA/+};mtHand2^{Cre}* model had micrognathia and microglossia, with the tongue positioned inferiorly to the developing palatal shelves. Without the tongue malpositioned between the palatal shelves during elevation, the palatal shelves developed and fused to form a normal palate with no cleft. Indeed, in the *R26R^{DTA/+};mtHand2^{Cre}* embryos that developed a cleft palate (N=3/8), the tongue was malpositioned between the palatal shelves. There was variation in the mandible and tongue size in the *R26R^{DTA/+};mtHand2^{Cre}* model, which may have accounted for the differences in mandible/tongue position and cleft status. Furthermore, we cannot discount that there may have been cell death with *mtHand2^{Cre}* expression in the anterior palatal shelf contributing to cases of cleft palate in the *R26R^{DTA/+};mtHand2^{Cre}* embryos. Additional experiments are required to assess the specific pattern of apoptosis and variability in mandible and tongue morphology and malposition in the *R26R^{DTA/+};mtHand2^{Cre}* model. Overall, these data highlight the importance of mandible and tongue shape and position in normal palate development, suggesting the retruded tongue position in between the palatal shelves contributes significantly to cleft palate (Figure 6).

In this study, we generated a new tool to study craniofacial development, *mtHand2^{Cre}*, with Cre recombinase expression specific to the mandibular mesenchyme. We utilized this new mouse reagent to model PRS with the loss of *Sox9* specifically in the mandibular mesenchyme, and showed *Sox9* is necessary for MC elongation and proper mandibular osteogenesis. Moreover,

we provide direct, genetic evidence that the mandibular malformation contributed to tongue malposition and cleft palate in the PRS mouse model.

FIGURES:

Figure 1. *mtHand2*^{Cre} is specifically expressed in the mandibular mesenchyme. (A-C) Images of freshly dissected *R26R^{mT/+};mtHand2^{Cre}* embryos show GFP (green) expression, indicating Cre recombination, in the first pharyngeal arch at E10.5 (A) and in the mandible at E14.5 (B) and E18.5 (C). Tissue not expressing Cre expresses RFP (red). (D-F") Coronal sections stained with antibody against GFP (green) and Dapi (blue) show GFP expressed throughout the embryo in the developing tongue and mandible at E12.5 (D'-D"). At E14.5, GFP was expressed in the tongue, Meckel's cartilage (MC, demarcated by white dashed circle), and developing mandibular bone (E-E"). GFP was expressed in ~50% of the chondrocytes in the MC and strongly expressed in the perichondrium. Of note, GFP staining was also noted in the anterior palatal shelves (yellow arrows) and nasal cartilage (pink arrows) at E14.5 (E). At E18.5, GFP expression was specific to the tongue, MC, and mandible (F-F"). There was no GFP expression in the dental mesenchyme of the developing molar (marked by white asterisk) at E14.5 (E') or E18.5 (F'), however, GFP was expressed in the incisor mesenchyme at E18.5 (F, white star). There were very few GFP expressing cells in the developing bones of the secondary palate at E18.5 (F-F", white arrows). Scale bar=500µm

Figure 2. The mandibular bone is dysmorphic and mineralization is disrupted in the *Sox9^{fl/fl};mtHand2^{Cre}* embryos compared to control. (A,B) Isosurfaces of the mandible and cranium from *Sox9^{fl/fl};mHand2^{Cre}* mutant (red) and *Sox9^{fl/fl}* control (blue) embryos at E18.5 show the mandible was small, dysmorphic, and retrognathic in the mutant compared to control. (C) The principal component analysis (PCA) plot shows *Sox9^{fl/fl};Hand2^{Cre}* and control mandibles separate significantly across PC1 and PC2. 90% confidence ellipses shown. (D) The wireframes of PC1 Min (blue), PC1 Max (red), and Average (gray dashed line) represent the shape differences in the

antero-posterior length, dorso-ventral width, and condylar and angular process angulation. (E,F) Relative mineral bone density maps show *Sox9^{fl/fl};mtHand2^{Cre}* mandibles had decreased bone volume and differences in bone density compared to control.

Figure 3. Loss of *Sox9* in the mandibular mesenchyme results in Meckel's cartilage truncation with decreased proliferation and misexpression of chondrogenic and osteogenic markers in the developing mandibular bone. (A-D) Images of skeletal preps show significant decrease in length of the Meckel's cartilage (MC) in *Sox9^{fl/fl};mtHand2^{Cre}* embryos compared to control at E13.5 and E14.5. Scale bar=500 μ m (E-J) Images of coronal sections of the MC (demarcated by white dashed circle) stained with antibody against BrdU (green), TUNEL (red), and Dapi (blue) show significant decrease in BrdU+/proliferative cells in the MC of *Sox9^{fl/fl};mtHand2^{Cre}* embryos at E12.5 (E,F), E13.5 (G,H), and E14.5 (I,J). TUNEL+/apoptotic cells were located primarily in the perichondrium (outlined by the yellow dashed circle), and there were more at E12.5 compared to E13.5 and E14.5 in both mutant and control. Scale bar=500 μ m (K) Measurements of the MC in skeletal preps show significant decrease in mutant compared to control at E13.5 and E14.5. (L) Quantification of %BrdU+/Dapi in the area of the MC show a significant decrease in mutant compared to control at each timepoint. (M-T) Images of coronal sections stained with RNA Scope probes (red) at E14.5. *Col2a1* was expressed in the MC (demarcated by black dashed circle) in control (M) and completely absent in *Sox9^{fl/fl};mtHand2^{Cre}* embryos (N). *Runx2* was expressed in the developing mandibular bone only in control (O, black arrowheads) while the *Runx2* expression area was increased to the medial aspect of the mandibular bone/MC in the mutant (P, white arrowheads). *Sp7* showed decreased expression in the *Sox9^{fl/fl};mtHand2^{Cre}* mandibular bone (R) compared to control (Q). *Ibsp* was expressed strongly in control (S) while expression in the *Sox9^{fl/fl};mtHand2^{Cre}* mandibular bone was significantly decreased and limited to the dorsal aspect compared to control. Scale bar=100 μ m

Figure 4. Loss of *Sox9* in the mandibular mesenchyme only results in palatal shelf elevation delay and cleft of the secondary palate. (A-F") Images of H&E stained coronal

sections of the developing palate and mandible in the anterior, middle, and posterior regions. (A-B") At E13.5, the palatal shelves in the *Sox9^{fl/fl};mtHand2^{Cre}* and *Sox9^{fl/fl}* control embryos appeared similar, oriented in the vertical position, lateral to the developing tongue. At E14.5, while the palatal shelves elevated and adhered with the medial epithelial seam (white arrow) present in control (C-C"), the palatal shelves were in the vertical position, not elevated, and the tongue was in the interpalatal shelf space in the mutant (D-D"). Of note, Meckel's cartilage (demarcated by black arrowheads) was present in the middle and posterior regions in the control (A'-A", C'-C") and only in the posterior region in the mutant (B", D"), showing the MC was short. (E-F") At E16.5, the palate was fused and bones were developing in the control (E-E"), and there was a cleft along the entire axis in the mutant with the tongue in the interpalatal shelf space (F-F"). Scale bar=500µm. (G) Graph showing a significant delay in palatal shelf elevation in mutant (MUT) embryos with most palatal shelves in the vertical (purple) position compared to the control (CON) in which most palatal shelves were in the adhered/fused (gray) or horizontal (orange) position. (H) Graph of the distance measured between the dorsal surface of the tongue and cranial base in the posterior (marked by dashed line in E") or nasal floor in the middle and anterior regions (marked by dashed line in E, E') shows a significant decrease in mutant (light blue) vs control (dark blue) in the anterior (ant), middle (mid), and posterior (post) palate at E16.5. *p<0.05

Figure 5. Micrognathia and microglossia in the *R26R^{DTA/+};mtHand2^{Cre}* embryos results in an inferior tongue position and fusion of the palate. (A,B) Sagittal images of embryo heads show the mandible (marked by red line) was severely retrognathic in the *R26R^{DTA/+};mtHand2^{Cre}* embryo (A) compared to control (B) at E16.5. (C-E") At E16.5, the palatal shelves were fused the control (C-C"). In the majority of *R26R^{DTA/+};mtHand2^{Cre}* embryos, the palate was fused with the small tongue positioned inferiorly (D-D", N=5/8). In N=3/8 of the *R26R^{DTA/+};mtHand2^{Cre}* embryos, there was a cleft of the secondary palate (E-E"). Scale bar=500µm

Figure 6. Both the mandible and tongue shape and position contribute to cleft palate. Outlines of coronal and sagittal sections of control, *Sox9^{fl/fl};mHand2^{Cre}*, and *R26R^{DTA/+};mHand2^{Cre}*

at E14.5 show the importance of both the mandible and tongue size and position during palatogenesis. In control, with a normal sized and positioned mandible and tongue, the palatal shelves fuse, and there is no cleft. With a small mandible and normal sized tongue in the *Sox9^{fl/fl};mtHand2^{Cre}* embryo, the tongue is positioned between the palatal shelves which do not elevate and fuse, resulting in cleft palate. With a small mandible and small tongue, the palatal shelves fuse, and there is no cleft in the majority of samples (N=5/8, no cleft). V=ventricle; B=brain; E=eye; NC=nasal cartilage; PS=palatal shelf; TB=tooth bud; MC=meckel's cartilage; T=tongue; CB=cranial base; NS=nasal septum; M=mandible.

Supplemental Figure 1. Sox9 is specifically deleted in the mandibular mesenchyme in *Sox9^{fl/fl};mtHand2^{Cre}* embryos. (A-D) Images of coronal sections stained with antibody against Sox9 (green) and Dapi (blue) show, at E12.5, Sox9 was expressed in *Sox9^{fl/fl}* control embryos in the region of the developing Meckel's cartilage (MC, white arrowheads) and cranial base (orange arrowheads) in the posterior (A) and middle (C) regions. There were also a few Sox9 expressing cells in the palatal shelves (C, asterisk). In *Sox9^{fl/fl};mtHand2^{Cre}* embryos, Sox9 expression was present in the cranial base and palatal shelves, but there was no Sox9 expressed in the MC (B,D), showing deletion was mandibular specific. (E-G') At E14.5, Sox9 was expressed in the cranial base (E, orange arrowheads), nasal cartilages (F, yellow arrowheads), molar dental epithelium (F', pink arrowhead), and the MC (E',F'). In the *Sox9^{fl/fl};Hand2^{Cre}* embryos, Sox9 was present in the cranial base (D), nasal cartilages (G), and molar epithelium (G'), but absent from the MC (D', G'). Scale bar=500µm

Supplemental Figure 2. The mandibular bone was significantly smaller in the *Sox9^{fl/fl};mtHand2^{Cre}* embryos compared to control. (A) Graph shows that the centroid size was significantly decreased in *Sox9^{fl/fl};mtHand2^{Cre}* embryos (light blue) compared to control (dark blue), revealing the E18.5 mandibular bone was significantly smaller in mutant compared to control. *p<0.05

Supplemental Figure 3. The area of the Meckel's cartilage (MC) was significantly decreased at all timepoints, and apoptosis was significantly decreased in the MC area at E13.5 in the *Sox9^{fl/fl};mtHand2^{Cre}* embryos compared to control. (A) Graph shows the Meckel's cartilage (MC) area was significantly decreased in *Sox9^{fl/fl};mtHand2^{Cre}* embryos (light blue) compared to control (dark blue) at E12.5, E13.5, and E14.5. *p<0.001 (B) Graph shows the %TUNEL+cells/MC area was significantly decreased in the *Sox9^{fl/fl};mtHand2^{Cre}* embryos compared to control at E13.5 only. Overall, the percentage of apoptotic cells was low. *p<0.05

Supplemental Figure 4. Loss of *Sox9* in the mandibular mesenchyme results in decreased expression of chondrogenic markers early in development. (A-D) Images of condensing mandibular mesenchyme stained with RNAscope probe against *Col2a1* and *Runx2* (red dots) at E12.5. (A,B) *Col2a1* was expressed in the condensing mesenchyme region where Meckel's cartilage will form in control (A, marked by yellow arrowheads) and significantly decreased in the same region in the *Sox9^{fl/fl};mtHand2^{Cre}* mutant (B). Expression of *Runx2* was similar in control (C) and mutant (D) at E12.5. Scale bar=100µm

Supplemental Figure 5. Loss of *Sox9* in the mandibular mesenchyme results in cleft of the secondary palate. (A,B) Ventral images of isosurfaces of E18.5 *Sox9^{fl/fl}* control (A) and *Sox9^{fl/fl};mtHand2^{Cre}* mutant (B) embryos show the bones of the secondary palate (palatine processes of the palatine and maxillary bones, highlighted in yellow) are fused in the control (A) and separated due to a complete cleft of the secondary palate in the mutant (B).

Supplemental Figure 6. Loss of *Sox9* in the mandibular mesenchyme results in cleft palate that persists until birth. (A,B) Images of H&E stained coronal sections show the palate fused in control (A) and a complete cleft of the secondary palate (marked by arrow) in the *Sox9^{fl/fl};mtHand2^{Cre}* embryo (B) at birth/postnatal day 0. Of note, the tongue in the *Sox9^{fl/fl};mtHand2^{Cre}* embryo mimics the cleft shape, suggesting the tongue was in the cleft space at birth. Scale bar=500µm

Supplemental Figure 7. *R26R^{DTA/+};mtHand2^{Cre}* embryos have micrognathia and microglossia and no other gross defects outside of the craniofacial complex. (A,B) Sagittal images of whole dissected embryos show the mandible (demarcated by red capped line) was severely retrognathic in the *R26R^{DTA/+};mtHand2^{Cre}* embryo (A) compared to control (B) at E15.5. The rest of the body, outside the craniofacial complex, was grossly normal in *R26R^{DTA/+};mtHand2^{Cre}* embryos compared to control.

ACKNOWLEDGEMENTS: A special thank you to Dr. David Clouthier. This work was supported by NIDCR K08DE028011, AAOF BRA, and BMRC Fellowship to A.F. Goodwin.

REFERENCES:

1. Caouette-Laberge, L., Bayet, B., and Larocque, Y. (1994). The Pierre Robin sequence: review of 125 cases and evolution of treatment modalities. *Plast. Reconstr. Surg.* 93, 934–942.
2. Karempelis, P., Hagen, M., Morrell, N., and Roby, B.B. (2020). Associated syndromes in patients with Pierre Robin Sequence. *Int. J. Pediatr. Otorhinolaryngol.* 131, 109842. 10.1016/j.ijporl.2019.109842.
3. Stoll, C., Alembick, Y., and Roth, M.P. (2023). Associated anomalies in Pierre Robin sequence. *Am. J. Med. Genet. A* 191, 2312–2323. 10.1002/ajmg.a.63344.
4. Benko, S., Fantès, J.A., Amiel, J., Kleinjan, D.-J., Thomas, S., Ramsay, J., Jamshidi, N., Essafi, A., Heaney, S., Gordon, C.T., et al. (2009). Highly conserved non-coding elements on either side of SOX9 associated with Pierre Robin sequence. *Nat. Genet.* 41, 359–364. 10.1038/ng.329.
5. Gordon, C.T., Attanasio, C., Bhatia, S., Benko, S., Ansari, M., Tan, T.Y., Munnich, A., Pennacchio, L.A., Abadie, V., Temple, I.K., et al. (2014). Identification of novel craniofacial regulatory domains located far upstream of SOX9 and disrupted in Pierre Robin sequence. *Hum. Mutat.* 35, 1011–1020. 10.1002/humu.22606.
6. Maroteaux, P., Spranger, J., Opitz, J.M., Kucera, J., Lowry, R.B., Schimke, R.N., and Kagan, S.M. (1971). [The campomelic syndrome]. *Presse Med.* 79, 1157–1162.
7. Zaballa, K., Singh, J., and Waters, K. (2023). The management of upper airway obstruction in Pierre Robin Sequence. *Paediatr. Respir. Rev.* 45, 11–15. 10.1016/j.prrv.2022.07.001.

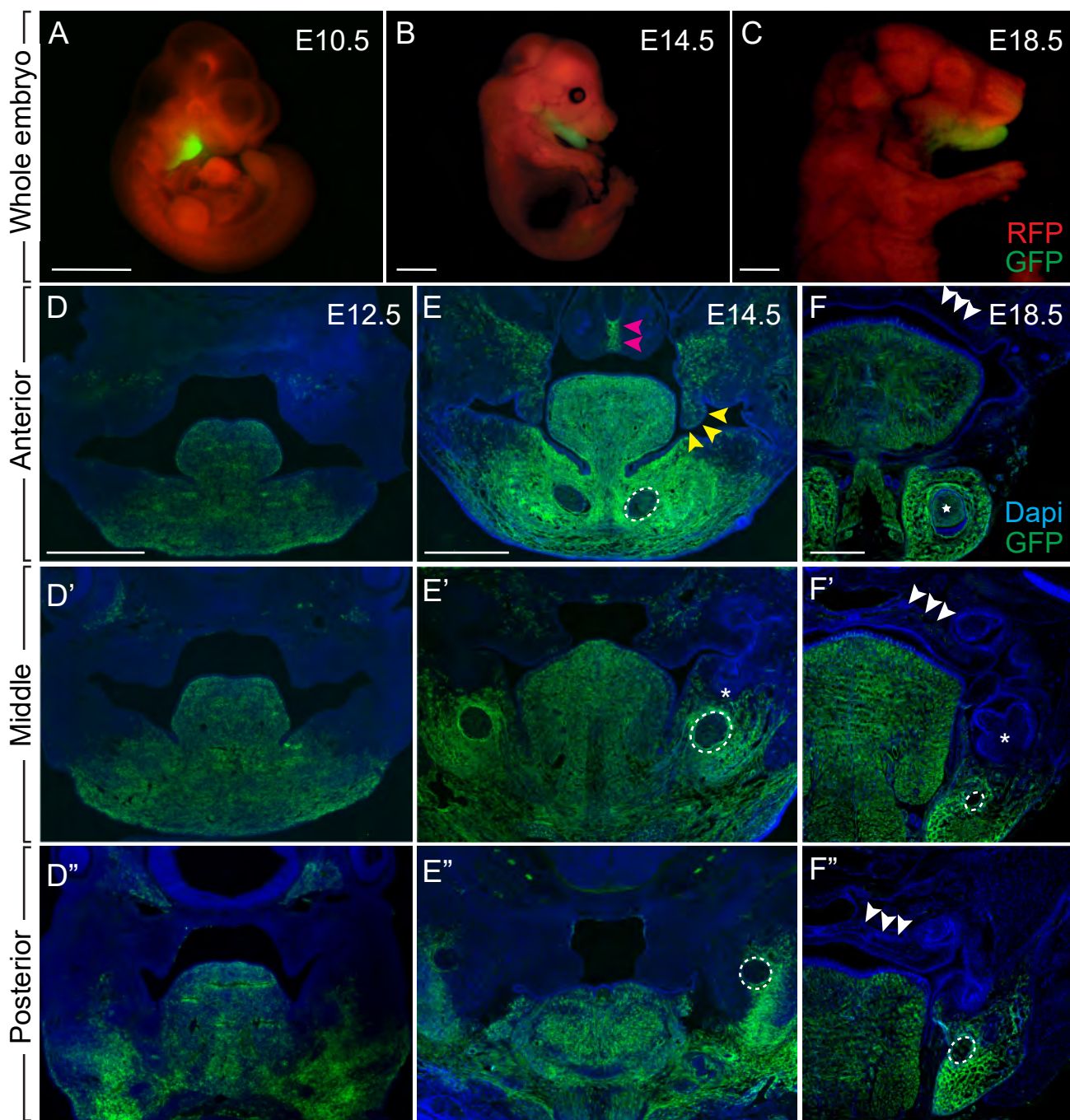
8. Evans, K.N., Sie, K.C., Hopper, R.A., Glass, R.P., Hing, A.V., and Cunningham, M.L. (2011). Robin sequence: from diagnosis to development of an effective management plan. *Pediatrics* 127, 936–948. 10.1542/peds.2010-2615.
9. Morrison, K.A., Collares, M.V., and Flores, R.L. (2021). Robin sequence: neonatal mandibular distraction. *Clin. Plast. Surg.* 48, 363–373. 10.1016/j.cps.2021.03.005.
10. Bush, J.O., and Jiang, R. (2012). Palatogenesis: morphogenetic and molecular mechanisms of secondary palate development. *Development* 139, 231–243. 10.1242/dev.067082.
11. Ferguson, M.W. (1988). Palate development. *Development* 103 *Suppl*, 41–60. 10.1242/dev.103.Supplement.41.
12. Trichilis, A., and Wroblewski, J. (1997). Expression of p53 and hsp70 in relation to apoptosis during Meckel's cartilage development in the mouse. *Anat. Embryol.* 196, 107–113. 10.1007/s004290050083.
13. Harada, Y., and Ishizeki, K. (1998). Evidence for transformation of chondrocytes and site-specific resorption during the degradation of Meckel's cartilage. *Anat. Embryol.* 197, 439–450. 10.1007/s004290050155.
14. Yang, R.-T., Zhang, C., Liu, Y., Zhou, H.-H., and Li, Z.-B. (2012). Autophagy prior to chondrocyte cell death during the degeneration of Meckel's cartilage. *Anat Rec (Hoboken)* 295, 734–741. 10.1002/ar.22433.
15. Dudas, M., Sridurongrit, S., Nagy, A., Okazaki, K., and Kaartinen, V. (2004). Craniofacial defects in mice lacking BMP type I receptor *Alk2* in neural crest cells. *Mech. Dev.* 121, 173–182. 10.1016/j.mod.2003.12.003.
16. Parada, C., Han, D., Grimaldi, A., Sarrión, P., Park, S.S., Pelikan, R., Sanchez-Lara, P.A., and Chai, Y. (2015). Disruption of the ERK/MAPK pathway in neural crest cells as a potential cause of Pierre Robin sequence. *Development* 142, 3734–3745. 10.1242/dev.125328.
17. Chen, Y., Wang, Z., Chen, Y., and Zhang, Y. (2019). Conditional deletion of *Bmp2* in cranial neural crest cells recapitulates Pierre Robin sequence in mice. *Cell Tissue Res.* 376, 199–210. 10.1007/s00441-018-2944-5.
18. Bi, W., Huang, W., Whitworth, D.J., Deng, J.M., Zhang, Z., Behringer, R.R., and de Crombrughe, B. (2001). Haploinsufficiency of *Sox9* results in defective cartilage primordia and premature skeletal mineralization. *Proc Natl Acad Sci USA* 98, 6698–6703. 10.1073/pnas.111092198.
19. Mori-Akiyama, Y., Akiyama, H., Rowitch, D.H., and de Crombrughe, B. (2003). *Sox9* is required for determination of the chondrogenic cell lineage in the cranial neural crest. *Proc Natl Acad Sci USA* 100, 9360–9365. 10.1073/pnas.1631288100.
20. Huang, X., Goudy, S.L., Ketova, T., Litingtung, Y., and Chiang, C. (2008). *Gli3*-deficient mice exhibit cleft palate associated with abnormal tongue development. *Dev. Dyn.* 237, 3079–3087. 10.1002/dvdy.21714.

21. Economou, A.D., Ohazama, A., Porntaveetus, T., Sharpe, P.T., Kondo, S., Basson, M.A., Gritli-Linde, A., Cobourne, M.T., and Green, J.B.A. (2012). Periodic stripe formation by a Turing mechanism operating at growth zones in the mammalian palate. *Nat. Genet.* *44*, 348–351. 10.1038/ng.1090.
22. Morgan, J.D., and Green, J.B.A. (2022). Methods of palate culture in later palatogenesis: elevation, horizontal outgrowth, and fusion. *Methods Mol. Biol.* *2403*, 63–80. 10.1007/978-1-0716-1847-9_6.
23. Brault, V., Moore, R., Kutsch, S., Ishibashi, M., Rowitch, D.H., McMahon, A.P., Sommer, L., Boussadia, O., and Kemler, R. (2001). Inactivation of the beta-catenin gene by Wnt1-Cre-mediated deletion results in dramatic brain malformation and failure of craniofacial development. *Development* *128*, 1253–1264. 10.1242/dev.128.8.1253.
24. Lewis, A.E., Vasudevan, H.N., O'Neill, A.K., Soriano, P., and Bush, J.O. (2013). The widely used Wnt1-Cre transgene causes developmental phenotypes by ectopic activation of Wnt signaling. *Dev. Biol.* *379*, 229–234. 10.1016/j.ydbio.2013.04.026.
25. Lan, Y., Wang, Q., Ovitt, C.E., and Jiang, R. (2007). A unique mouse strain expressing Cre recombinase for tissue-specific analysis of gene function in palate and kidney development. *Genesis* *45*, 618–624. 10.1002/dvg.20334.
26. Sun, C., Zhang, T., Liu, C., Gu, S., and Chen, Y. (2013). Generation of Shox2-Cre allele for tissue specific manipulation of genes in the developing heart, palate, and limb. *Genesis* *51*, 515–522. 10.1002/dvg.22397.
27. Ruest, L.-B., Dager, M., Yanagisawa, H., Charité, J., Hammer, R.E., Olson, E.N., Yanagisawa, M., and Clouthier, D.E. (2003). dHAND-Cre transgenic mice reveal specific potential functions of dHAND during craniofacial development. *Dev. Biol.* *257*, 263–277. 10.1016/s0012-1606(03)00068-x.
28. Muzumdar, M.D., Tasic, B., Miyamichi, K., Li, L., and Luo, L. (2007). A global double-fluorescent Cre reporter mouse. *Genesis* *45*, 593–605. 10.1002/dvg.20335.
29. Akiyama, H., Chaboissier, M.-C., Martin, J.F., Schedl, A., and de Crombrughe, B. (2002). The transcription factor Sox9 has essential roles in successive steps of the chondrocyte differentiation pathway and is required for expression of Sox5 and Sox6. *Genes Dev.* *16*, 2813–2828. 10.1101/gad.1017802.
30. Voehringer, D., Liang, H.-E., and Locksley, R.M. (2008). Homeostasis and effector function of lymphopenia-induced “memory-like” T cells in constitutively T cell-depleted mice. *J. Immunol.* *180*, 4742–4753. 10.4049/jimmunol.180.7.4742.
31. Motch Perrine, S.M., Wu, M., Stephens, N.B., Kriti, D., van Bakel, H., Jabs, E.W., and Richtsmeier, J.T. (2019). Mandibular dysmorphology due to abnormal embryonic osteogenesis in FGFR2-related craniosynostosis mice. *Dis. Model. Mech.* *12*. 10.1242/dmm.038513.
- 32.
33. Akiyama, H., Kim, J.-E., Nakashima, K., Balmes, G., Iwai, N., Deng, J.M., Zhang, Z., Martin, J.F., Behringer, R.R., Nakamura, T., et al. (2005). Osteo-chondroprogenitor cells

are derived from Sox9 expressing precursors. *Proc Natl Acad Sci USA* 102, 14665–14670. 10.1073/pnas.0504750102.

34. Dy, P., Wang, W., Bhattaram, P., Wang, Q., Wang, L., Ballock, R.T., and Lefebvre, V. (2012). Sox9 directs hypertrophic maturation and blocks osteoblast differentiation of growth plate chondrocytes. *Dev. Cell* 22, 597–609. 10.1016/j.devcel.2011.12.024.

Figure 1.



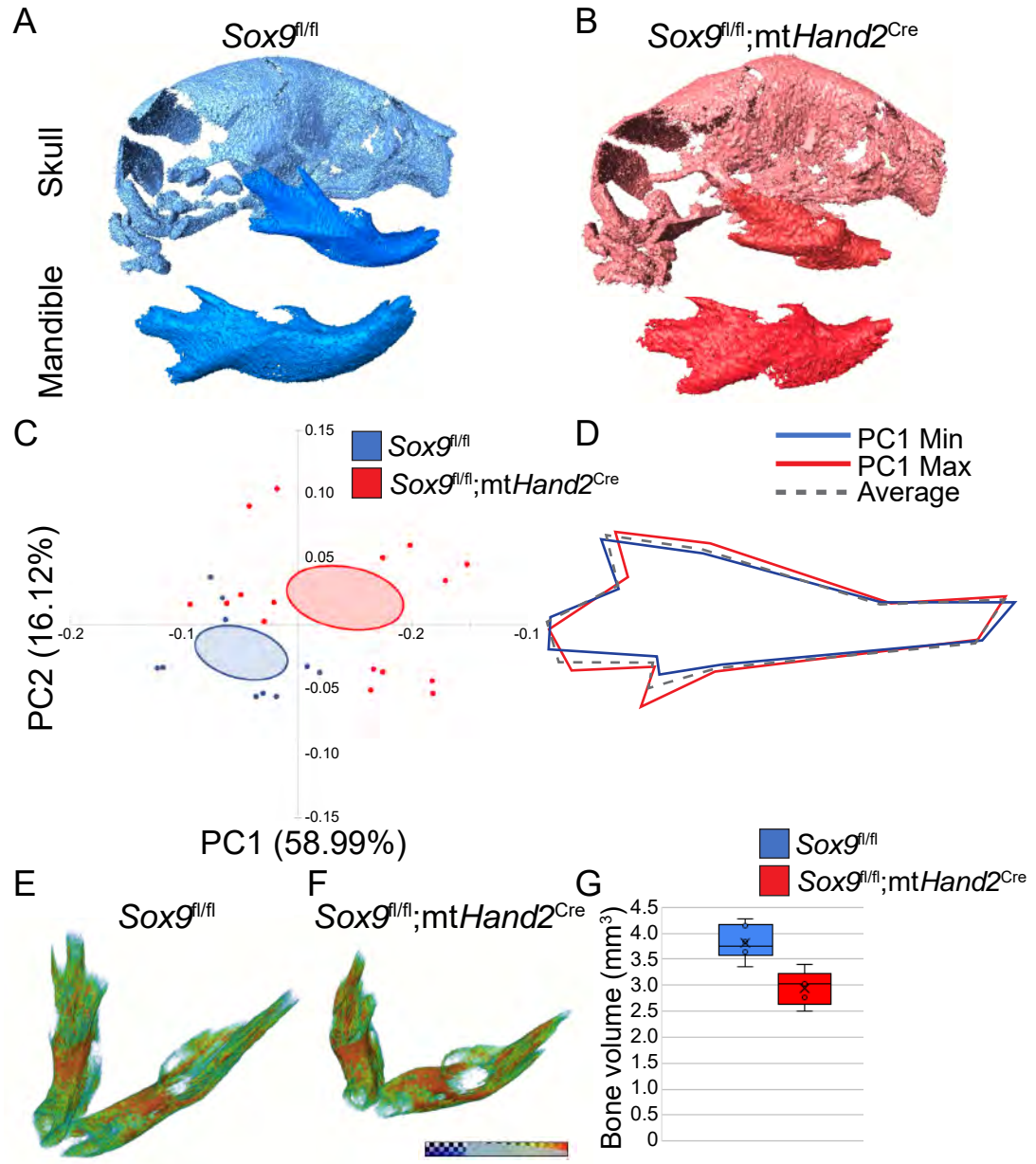
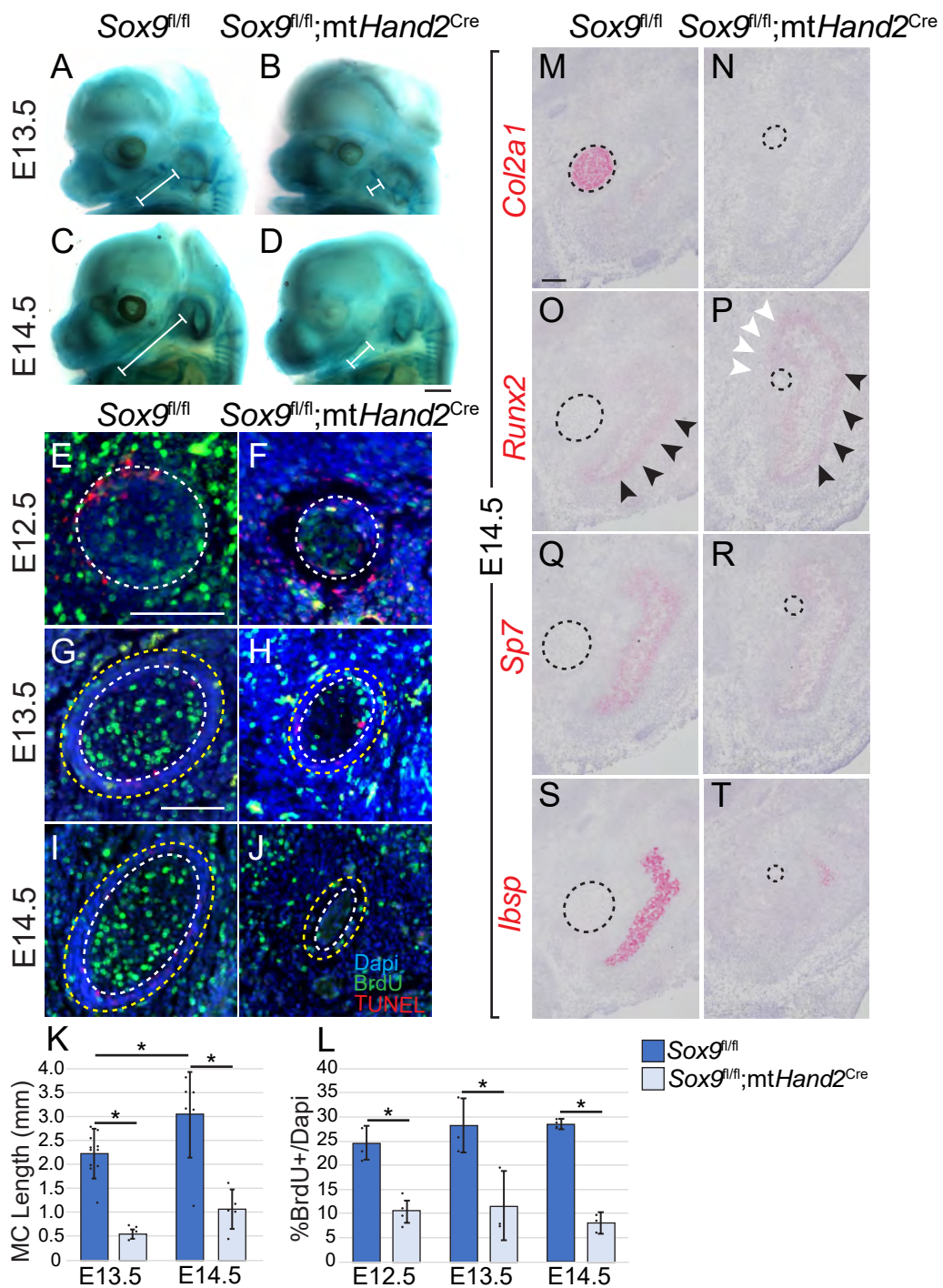


Figure 3.



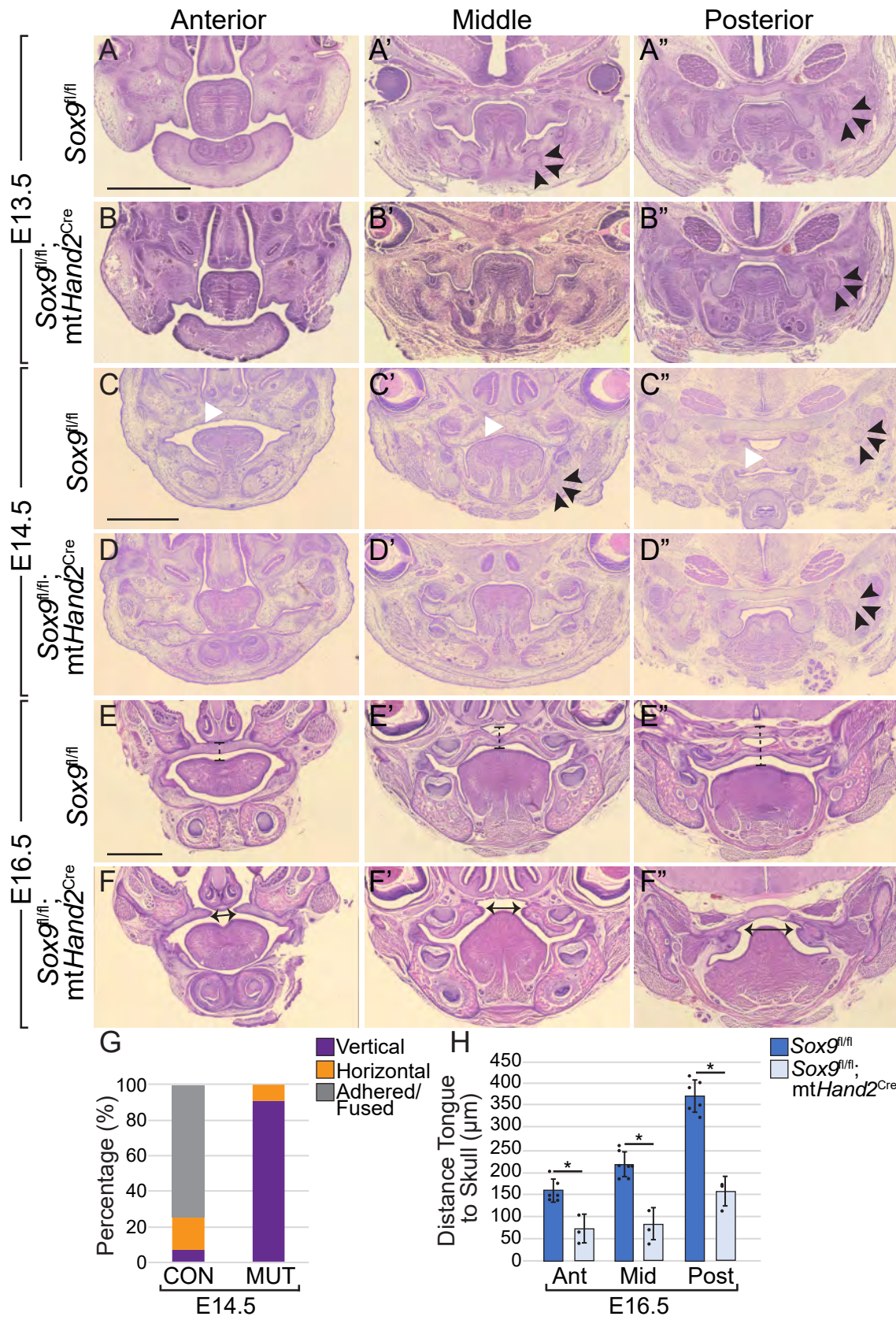


Figure 5.

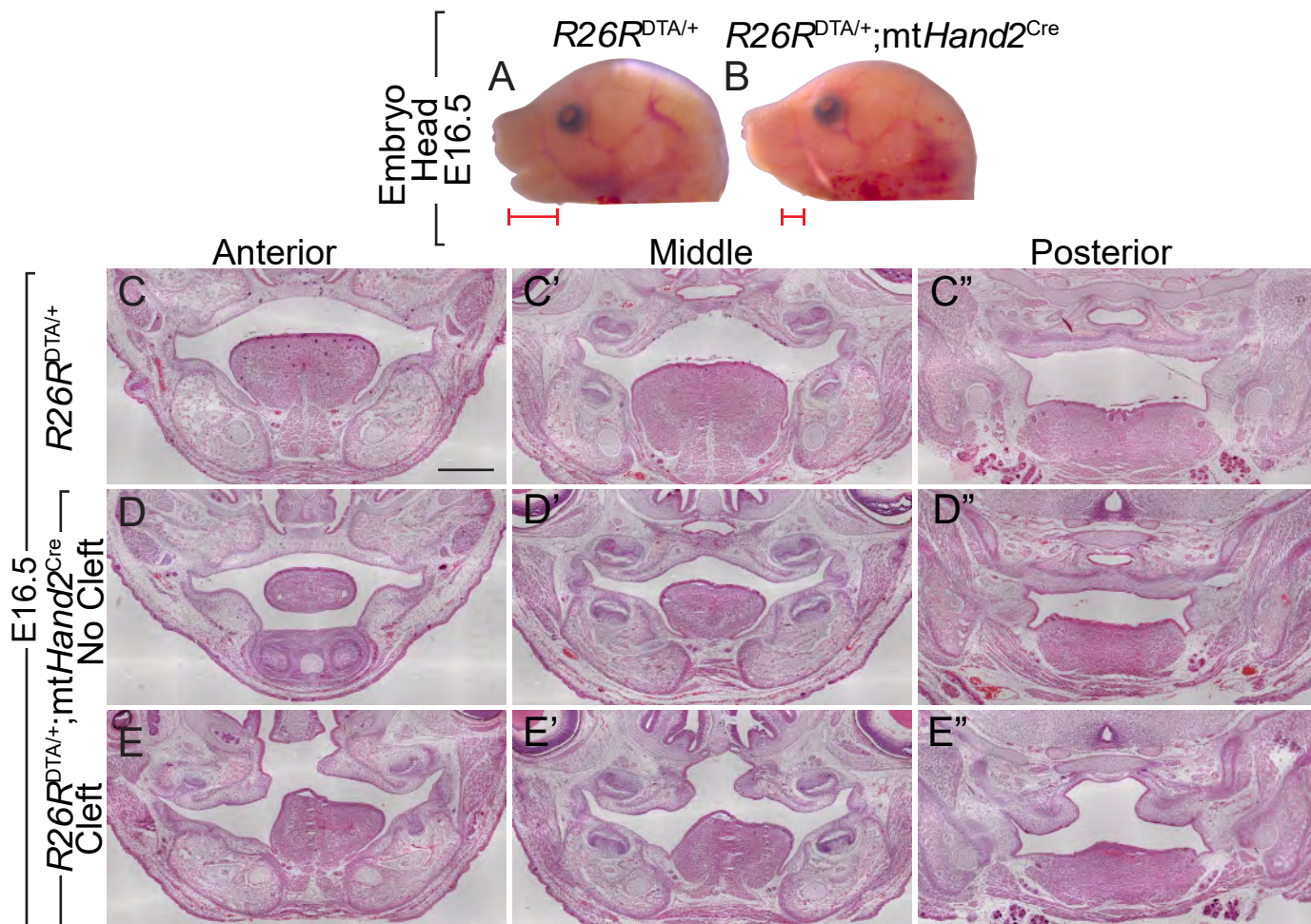
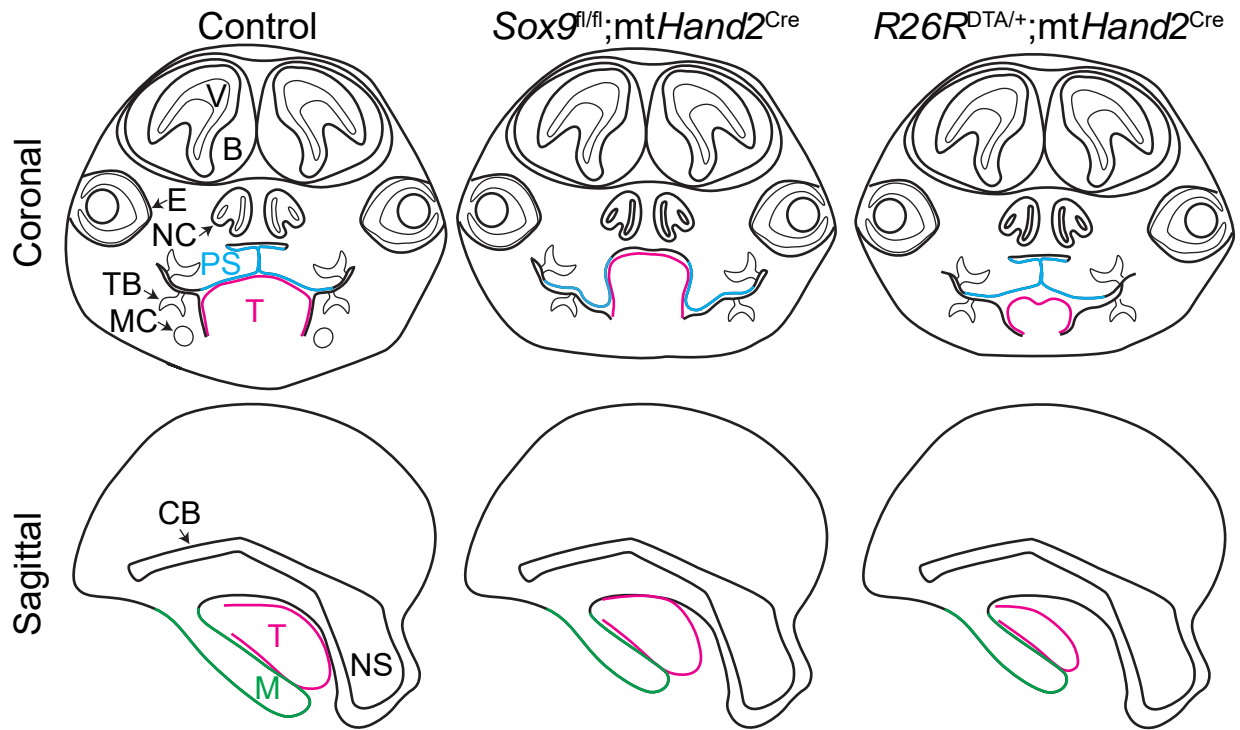


Figure 6.



Mandible Size	Normal	Small	Small
Tongue Size	Normal	Normal	Small
Cleft Palate	0%	100%	38%

